BIOCELL

Tech Science Press

http://doi.org/10.32604/biocell.2026.075139

ARTICLE

Anti-Inflammatory Effects of Veratramine against Lipopolysaccharide-Induced Inflammation

Gyuri Han[#], Yun Hee Jeong[#], Ga Eun Kim and Jong-Sup Bae[*]

College of Pharmacy, CMRI Research Institute of Pharmaceutical Sciences, Kyungpook National University, Daegu, Republic of Korea

*Corresponding Author: Jong-Sup Bae. Email: baejs@knu.ac.kr

[#]These authors contributed equally to this work as the first author

Received: 25 October 2025; Accepted: 28 January 2026; Published: 13 May 2026

ABSTRACT: Objectives: Plant-derived bioactive molecules are increasingly recognized as valuable therapeutic resources for managing diverse pathological conditions, particularly those involving vascular inflammation. This study aimed to determine whether veratramine (VRT), a naturally occurring steroidal alkaloid found in Veratrum species of the Liliaceae family, attenuates LPS-induced vascular and pulmonary inflammation by upregulating heme oxygenase-1 (HO-1) and modulating the Nrf2, nuclear factor (NF)-κB, and signal transducer and activator of transcription (STAT1) signaling pathways. **Methods**: The study assessed the modulatory effects of VRT on HO-1, cyclooxygenase-2 (COX-2), and inducible nitric oxide synthase (iNOS) in LPS-activated human umbilical vein endothelial cells (HUVECs), as well as on iNOS, tumor necrosis factor-α (TNF-α), and interleukin-1β (IL-1β) expression in LPS-treated mice. The VRT doses (0.06–0.6 mg/kg) in mice were chosen to approximate peripheral concentrations of 2–20 μM, corresponding to the non-cytotoxic, anti-inflammatory range in HUVECs, based on calculations using mouse blood volume and body weight, and no overt acute toxicity was observed at these doses in this model. **Results**: Treatment with VRT enhanced HO-1 induction, inhibited NF-κB activation, diminished COX-2/PGE_2 and iNOS/NO production, and attenuated STAT1 phosphorylation. In addition, VRT promoted nuclear translocation of Nrf2 and its binding to antioxidant response elements (AREs), thereby suppressing IL-1β expression in HUVECs. The VRT-mediated inhibition of iNOS/NO was abolished by HO-1 silencing through RNA interference. *In vivo*, VRT markedly reduced iNOS expression in lung tissue and lowered TNF-α levels in bronchoalveolar lavage fluid. **Conclusion**: Altogether, these findings demonstrate that VRT exhibits substantial anti-inflammatory potential and may serve as a promising candidate for managing inflammation-related vascular disorders.

KEYWORDS: Veratramine; endothelium; inducible nitric oxide synthase (iNOS); p-signal transducer and activator of transcription (STAT)-1

1 Introduction

Heme oxygenase-1 (HO-1) plays a pivotal role in defending tissues from inflammation-associated injury and excessive reactive oxygen species (ROS) accumulation, especially under pathological conditions such as autoimmune disorders, pulmonary diseases, and cancer [1,2]. By suppressing the synthesis of proinflammatory mediators—including tumor necrosis factor (TNF)-α, interleukin (IL)-1β, and IL-6—HO-1 contributes significantly to the resolution of inflammation [2]. Previous studies have confirmed the protective role of HO-1 in mitigating acute septic inflammation and vascular disorders associated with endothelial dysfunction [2,3]. The Keap1–Nrf2–antioxidant response element (ARE) signaling axis is

fundamental in modulating oxidative stress and counteracting inflammation by controlling genes responsible for detoxification and antioxidative defense [4]. Nrf2 serves as a master regulator of cytoprotective responses against environmental insults, positioning the Nrf2–ARE system as an important therapeutic target for inflammation-associated conditions [4,5]. Furthermore, both signal transducer and activator of transcription (STAT)1 and nuclear factor (NF)-κB represent core inflammatory signaling pathways [6,7]. Their activation promotes the production of proinflammatory factors that attract immune cells to damaged tissues [6,7]. However, aberrant or prolonged activation of these pathways contributes to chronic inflammation, tissue injury, and disease progression, emphasizing the potential of targeting STAT1 and NF-κB for the treatment of inflammation-related disorders.

Respiratory dysfunction in the lungs represents a severe pathological condition marked by extensive inflammation, which leads to proliferative edema, oxygen deprivation, and the formation of neutrophil extracellular traps within pulmonary tissues [8]. Lipopolysaccharide (LPS), a key endotoxin derived from gram-negative bacteria, acts as a primary trigger for inflammatory lung injury by activating transcriptional regulators that induce the release of pro-inflammatory mediators [8]. This sustained activation amplifies inflammatory signaling and contributes to the pathogenesis of chronic disorders such as endothelial dysfunction, asthma, chronic obstructive pulmonary disease (COPD), and cystic fibrosis [8].

Plant-derived natural compounds are increasingly recognized as promising and safer therapeutic alternatives to conventional synthetic anti-inflammatory drugs due to their minimal side effects and diverse pharmacological potential [9]. Among these bioactive molecules, veratramine (VRT)—a naturally occurring steroidal alkaloid isolated from several species of the Veratrum genus within the Liliaceae family—has garnered scientific interest [10]. Previous investigations revealed that veratramine exerts multiple physiological actions, including blood pressure regulation, sodium channel inhibition, and analgesic activity [11,12]. In addition, VRT exhibits a wide range of biological functions, such as anticancer, antihypertensive, and dermatological benefits [13–15]. Although Li et al. documented the anti-inflammatory capacity of veratramine, the molecular mechanisms underlying these effects remain insufficiently characterized [16]. This study addresses the mechanistic gap left by previous research by demonstrating that VRT exerts anti-inflammatory effects through upregulating HO-1 and modulating Nrf2, NF-κB, and STAT1 signaling pathways in both *in vitro* and *in vivo* models. Unlike earlier reports, such as Li et al. [16], which documented the anti-inflammatory potential of VRT without detailed pathway analysis, this study provides direct evidence of HO-1's pivotal role via RNA interference and comprehensive molecular assessments.

Therefore, the present study was designed to elucidate the influence of VRT on HO-1 expression and inflammatory mediators—including TNF-α, IL-1β, and NO—in LPS-stimulated HUVECs and in LPS-treated mouse models. This investigation aims to clarify the mechanistic involvement of VRT in modulating the HO-1 signaling cascade and suppressing inflammatory cytokines, thereby supporting its therapeutic potential in inflammation-related pathologies.

2 Materials and Methods

2.1 Cell Culture and Substances

In this experiment, HUVECs were sourced from Cambrex BioScience (C2517AT25; Charles City, IA, USA) and cultured in accordance with procedures outlined in a previous report [17]. All HUVEC cultures were routinely tested and confirmed to be free of mycoplasma contamination throughout the experiments. VRT (product No. PHL82679, purity > 98%), dexamethasone (Dex; positive control; D1756), LPS (from *Escherichia coli*; L2880), penicillin G (PENNA), streptomycin (S9137), and dimethyl

sulfoxide (DMSO, D8418) were all provided by Sigma Chemical Co. (St. Louis, MO, USA; catalog Nos. D1756, L2880, PENNA, S9137 and D8418, respectively). Human HO-1 siRNA (sc-35554, Sense: 5′-GAUGAAGAGUUGGAAGAAAtt-3′, Antisense: 5′-UUUCUUCCAACUCUUCAUCtt-3′) and control siRNA (sc-37007, Sense: 5′-UUCUCCGAACGUGUCACGUtt-3′, Antisense: 5′-ACGUGACACGUUCGGAGAAtt-3′) were obtained from Santa Cruz Biotechnology (Santa Cruz, CA, USA). HUVECs between passages 3 and 5 were plated (1×10^5 cells per 35 mm dish) and serum-deprived overnight before performing an enzyme-linked immunosorbent assay (ELISA). Some cultures were pre-incubated with LPS (1 μg/mL, 6 h) followed by VRT exposure for another 6 h, whereas others received only VRT for the same duration to evaluate HO-1 expression levels.

2.2 Mouse Model of LPS-Induced Lung Injury

Male C57BL/6 mice (6–7 weeks old, average body weight 27 g) were procured from Orient Bio Inc. (Seongnam, Republic of Korea). Before initiating experimental protocols, all animals were acclimated for 12 days to ensure physiological stabilization, in alignment with prior research [18,19]. An LPS-induced lung injury model was established by administering LPS at a dose of 15 mg/kg, as previously described in well-established experimental studies [20,21]. LPS (15 mg/kg) was administered intraperitoneally using 28-gauge needles, with 0.2% DMSO serving as the vehicle control. After 6 h, mice received an intravenous dose of VRT at concentrations ranging from 0.06 to 0.6 mg/kg (n = 5 per group). A total of 40 mice were divided into 8 groups (n = 5/group): Vehicle, VRT-only (0.61 mg/kg), LPS-only (15 mg/kg), four LPS+VRT groups (0.06, 0.15, 0.3, 0.61 mg/kg), and a positive control LPS+Dex group (LPS: 15 mg/kg; Dex: 0.61 mg/kg). All animal procedures were approved by the Institutional Animal Care and Use Committee of Kyungpook National University (IRB No. KNU 2022-112). Bronchoalveolar lavage fluid (BALF) was obtained by gently aspirating phosphate-buffered saline (PBS) through the trachea, followed by centrifugation at 1500× g for 10 min at 4°C. The supernatant was collected and stored at −80°C for later biochemical analyses. The experiment was conducted in accordance with the ARRIVE Essential 10 guidelines.

2.3 ELISA

To investigate the effect of VRT on HUVECs, cells were initially incubated with LPS (1 μg/mL) for 6 h and subsequently treated with VRT for another 6 h. In parallel, a separate group of cells was exposed solely to VRT for 6 h to determine HO-1 expression levels. The degree of STAT1 phosphorylation was quantified using ELISA kits from Abcam (ab126455, Cambridge, UK). Concentrations of prostaglandin E2 (PGE2, KGE004B), HO-1 (DYC3776-2), IL-1β (DLB50), TNF-α (QTA00B), and iNOS (DNS00) were measured with ELISA kits supplied by R&D Systems (Minneapolis, MN, USA), employing supernatants collected after cell culture centrifugation at 1500 × g for 10 min at 4°C for each analysis.

2.4 Cell Viability Assay

Cell viability was determined using the MTT assay in accordance with previously established methods [22,23]. HUVECs were plated at a density of 5×10^3 cells per well in 96-well plates and incubated with or without LPS (1 μg/mL) for 6 h. And then, cells were incubated with VRT (10 to 50 μM) for 48 h. Subsequently, the cells were rinsed and exposed for an additional 4 h after the addition of 100 μL of MTT solution (1 mg/mL) to each well. Formazan crystals generated during the reaction were dissolved in 150 μL of DMSO, and absorbance was measured at 570 nm using a Tecan Infinite M200 spectrophotometer (Tecan, Austria GmbH). The percentage of viable cells was calculated relative to the control group, with untreated cells defined as 100% viability.

2.5 Nitrite Levels

Nitric oxide production was quantified by determining nitrite (NO_2^-) concentrations within the culture medium. Equal volumes of Griess reagent from a commercial kit (Griess Assay Kit/Griess Reagent Kit, ab234044; Abcam, Cambridge, UK) and the collected culture supernatants (1:1, *v*/*v*; typically 50 µL supernatant mixed with 50 µL Griess reagent per well) were combined and incubated at room temperature for 10–15 min, according to the manufacturer's instructions. The absorbance of the resulting chromophore was then measured at 540 nm using a spectrophotometric microplate reader (Sunrise absorbance microplate reader, Tecan Austria GmbH, Grödig, Austria). All measurements were performed in triplicate to ensure reproducibility and data reliability.

2.6 Intracellular Fractionation, Immunoblotting, and Co-Coimmunoprecipitation (Co-IP)

- **Intracellular fractionation:** Cytosolic and nuclear extracts were prepared from treated HUVECs using a previously published fractionation protocol with stepwise lysis and differential centrifugation [24]. Lamin B and β-actin were used as internal controls for nuclear and cytosolic fractions, respectively, to verify fraction purity and equal loading. Briefly, HUVECs were harvested at 80–90% confluence, and intracellular fractionation was performed using $1–2 \times 10^6$ cells (corresponding to approximately 50–100 µg total protein) per condition.
- **Immunoblotting conditions:** Immunoblotting was performed using primary antibodies against iNOS (sc-651, 1:1000), COX-2 (sc-1747, 1:1000), lamin B (sc-6216, 1:1000), Keap1 (sc-365626, 1:1000), Nrf2 (sc-365949, 1:1000), and β-actin (sc-47778, 1:5000) (all from Santa Cruz Biotechnology, Santa Cruz, CA, USA; other antibodies as per the manufacturers' datasheets). Protein samples (20 µg total protein per lane) were separated by 10% SDS-PAGE and transferred to PVDF membranes. Membranes were blocked with 5% non-fat dry milk in Tris-buffered saline containing 0.1% Tween-20 (TBS-T) for 1 h at room temperature and then incubated with primary antibodies in blocking buffer overnight at 4°C. After washing with TBS-T, membranes were incubated with HRP-conjugated secondary antibodies (goat anti-mouse IgG-HRP, sc-2005, 1:5000; goat anti-rabbit IgG-HRP, sc-2004, 1:5000; Santa Cruz Biotechnology, Dallas, TX, USA) for 1 h at room temperature, and proteins were visualized using an enhanced chemiluminescence detection system. Densitometric analyses were performed on three independent biological experiments, each run with technical duplicate or triplicate lanes for confirmation.
- **Co-IP:** HUVECs were lysed in ice-cold lysis buffer (20 mM Tris-HCl, pH 7.5, 150 mM NaCl, 1 mM EDTA, 1% NP-40, 10% glycerol) supplemented with protease and phosphatase inhibitor cocktails (e.g., P8340 and P5726; Sigma-Aldrich) and centrifuged at 12,000× *g* for 10 min at 4°C to obtain clarified supernatants. Clarified lysates (typically 800 µg total protein per IP) were pre-cleared with protein A-agarose (Santa Cruz Biotechnology) for 1 h at 4°C. The pre-cleared lysates were then incubated with anti-Nrf2 antibody (1:100; Santa Cruz Biotechnology, sc-365949) or species-matched normal rabbit IgG control for 1 h at 4°C, followed by the addition of protein A-agarose and gentle rotation overnight at 4°C. Immunocomplexes were collected by centrifugation (5000× *g*, 3–5 min, 4°C), washed three times with lysis buffer (0.5–1 mL per wash), and eluted in reducing SDS sample buffer (62.5 mM Tris-HCl, pH 6.8, 2% SDS, 10% glycerol, 0.01% bromophenol blue, 5% β-mercaptoethanol or 50 mM DTT) by boiling for 10 min, then analyzed by immunoblotting using anti-Keap1 (sc-365626) and anti-Nrf2 (sc-365949) antibodies with appropriate HRP-conjugated secondary antibodies (goat anti-mouse IgG-HRP [Santa Cruz Biotechnology, sc-2005, 1:5000] and goat anti-rabbit IgG-HRP [Santa Cruz Biotechnology, sc-2004, 1:5000]).

2.7 Quantitative Real-Time-Polymerase Chain Reaction (qPT-PCR)

Total RNA was isolated using TRI Reagent Solution (TRI Reagent, AM9738; Invitrogen, Thermo Fisher Scientific) according to the manufacturer's instructions. RNA purity and concentration were assessed spectrophotometrically (A260/A280), and only samples with A260/A280 between 1.8 and 2.0 were used; typically, 1 μg of total RNA was used for first-strand cDNA synthesis in a 20 μL reaction. cDNA was synthesized in a 20 μL reaction mixture containing total RNA (1 μg), 0.5 μg/μL oligo(dT)-adapter primer (Invitrogen), 1× reverse transcription buffer, 0.5 mM each dNTP, 20–40 U RNase inhibitor, and M-MLV reverse transcriptase (Invitrogen), using a PX2 Thermal Cycler (Thermo Hybaid PX2, Thermo Fisher Scientific, Waltham, MA, USA). Reverse transcription was performed at 42°C for 60 min, followed by enzyme inactivation at 70°C for 10 min, and the resulting cDNA was diluted appropriately for subsequent qPCR. Quantitative real-time PCR was carried out in a 20 μL volume containing 10 μL of 2× SYBR Green PCR master mix, 0.4 μL each of forward and reverse primers (final 0.2 μM), 2 μL of cDNA template, and nuclease-free water. Reactions were run on a real-time PCR detection system (e.g., StepOnePlus or similar real-time PCR instrument, Applied Biosystems/Thermo Fisher Scientific) under the following cycling conditions: initial denaturation at 95°C for 10 min, followed by 40 cycles of 95°C for 15 s and 60°C for 60 s, with a melt curve analysis to verify product specificity. The relative expression levels of iNOS, COX-2, Nrf2, and HO-1 were normalized to β-actin as an internal reference gene. Relative mRNA expression was calculated using the $2^{-\Delta\Delta Ct}$ method, where ΔCt = Ct(target) − Ct(β-actin), ΔΔCt = ΔCt(sample) − ΔCt(control), and the relative expression (fold change) = $2^{-\Delta\Delta t}$.

The primer sequences used for qRT-PCR analysis were as follows: COX-2 forward: 5′-CCC CAT TAG CAG CCA GTT-3′, COX-2 reverse: 5′-CAT TCC CCA CGG TTT TGA-3′; iNOS forward: 5′-GTT CTC AGC CCA ACA ATA CAA GA-3′, iNOS reverse: 5′-GTG GAC GGG TCG ATG TCA C-3′; Nrf2 forward: 5′-TCC TAT GCG TGA ATC CCA AT-3′, Nrf2 reverse: 5′-GCG GCT TGA ATG TTT GTC TT-3′; HO-1 forward: 5′-GGG CTG TGA ACT CTG TCC AAT-3′, HO-1 reverse: 5′-GGT GAG GGA ACT GTG TCA GG-3′; and β-actin forward: 5′-TCG TGC GTG ACA TCA AAG A-3′, β-actin reverse: 5′-CAT ACC CAA GAA GGA AGG CT-3′.

2.8 Transfection

Plasmids containing the NF-κB-luciferase reporter construct (pGL4.32[luc2P/NF-κB-RE/Hygro]; Promega, Madison, WI, USA), ARE-luciferase reporter construct (pGL3-ARE), HO-1 siRNA (sc-35554; Santa Cruz Biotechnology, Dallas, TX, USA), and non-targeting control siRNA (sc-37007; Santa Cruz Biotechnology) were transfected into HUVECs (seeded at 70% confluency, ~3×10^5 cells/well in 12-well plates) using SuperFect transfection reagent (301307; QIAGEN, Hilden, Germany) at a DNA:reagent ratio of 1:4 (μg:μL) or siRNA:reagent ratio of 1:6 (pmol:μL). The expression experiments used a mammalian expression vector pcDNA™3.1(+) (Invitrogen, Thermo Fisher Scientific, Waltham, MA, USA; catalog no. V790-20), which carries the CMV promoter for high-level gene expression in mammalian cells. Transfection complexes were incubated with cells for 4 h in serum-free medium, after which the medium was replaced with fresh growth medium (EGM-2; Lonza, Walkersville, MD, USA; CC-3162). Efficiency was confirmed by qRT-PCR and Western blot showing >70% HO-1 knockdown.

2.9 ARE Luciferase Reporter Assay

For the ARE luciferase reporter assay, transfected HUVECs (seeded at 70% confluency, ~3×10^5 cells/well in 12-well plates) were gently rinsed with PBS and lysed in 200 μL Passive Lysis Buffer (5X PLB) from the Dual-Luciferase Reporter Assay System (E1910; Promega, Madison, WI, USA). Lysates (20 μL) were

transferred to a 96-well plate or tube, and luciferase activities were quantified using a TD-20/20 luminometer (Turner BioSystems, Sunnyvale, CA, USA) by adding 100 µL Luciferase Assay Reagent II (LAR II) for firefly luciferase (10 s delay/10 s integration), followed by 100 µL Stop & Glo® Reagent for Renilla luciferase. Renilla luciferase (pRL-TK vector, Promega; 0.02 µg/well) was cotransfected at a 10:1 ratio with the firefly reporter plasmid (0.2 µg/well) for normalization. Data were expressed as the ratio of firefly to Renilla luciferase activity from triplicate independent transfections.

2.10 Histopathological Analysis

Five mice received intraperitoneal injections of LPS, followed six hours later by intravenous administration of VRT at a dose of 0.6 mg/kg. Subsequently, the animals were euthanized, and lung tissues were collected for histopathological evaluation using hematoxylin and eosin (H&E) staining, as outlined in previous studies [25]. Pulmonary tissue damage was scored according to a standardized grading scale from 1 to 4 [24]. A score of 1 indicated minimal or no damage, while a score of 4 represented severe damage with widespread inflammatory cell infiltration and tissue destruction. The analysis was performed in a blinded manner to prevent observer bias, ensuring that the evaluator was unaware of the treatment groups during scoring.

2.11 Evaluation of Oxidative Stress Markers

HUVECs were lysed by sonication in ice-cold assay buffer, centrifuged (10,000× *g*, 10 min, 4°C), and supernatants quantified for protein (Bradford assay, Bio-Rad). Superoxide dismutase (SOD) activity was measured using SOD Assay Kit (19160; Sigma-Aldrich/Fluka, Buchs, Switzerland) at 550 nm (Sunrise microplate reader, Tecan Austria GmbH, Grödig, Austria), where 1 U = enzyme inhibiting 50% NBT reduction (U/mg protein). CAT activity was determined using Catalase Assay Kit (CAT100; Sigma-Aldrich, St. Louis, MO, USA) by monitoring ΔA240 nm decrease (1 U = 1 µmole H_2O_2/min at 25°C, U/mg protein), using the same spectrophotometer.

2.12 Statistical Analysis

Data were analyzed using GraphPad Prism software (version 9.0; GraphPad Software, San Diego, CA, USA). The results in the study are expressed as mean ± standard deviation (SD) based on three independent experiments. Group comparisons were conducted using one-way analysis of variance (ANOVA) followed by Tukey's post hoc test to identify statistically significant differences. A *p*-value less than 0.05 was considered indicative of statistical significance.

3 Results

3.1 Effect of VRT on iNOS and COX-2 Levels in LPS-Activated HUVECs

To investigate the influence of VRT on the expression of inflammation-associated genes, the study measured iNOS and COX-2, key mediators of the inflammatory response. HUVECs were exposed to LPS for 6 h, followed by treatment with various concentrations of VRT or with 20 µM Dex for an additional 6 h. Quantification through qPCR, ELISA, and immunoblot analyses showed that both VRT and Dex (20 µM) reduced LPS-induced expression of iNOS and COX-2 in a dose-dependent manner (Fig. 1A–D). Likewise, the production of their downstream molecules, PGE_2 and NO, was diminished upon VRT or Dex exposure (Fig. 1E,F). Cell viability analysis using the MTT assay revealed no significant reduction up to 50 µM VRT, confirming the absence of cytotoxicity in HUVECs (Fig. 1G). Furthermore, VRT treatment was found to

reduce LPS-associated cytotoxicity in these endothelial cells (Fig. 1G). Altogether, these results indicate that VRT inhibits iNOS expression and attenuates LPS-induced NO generation.

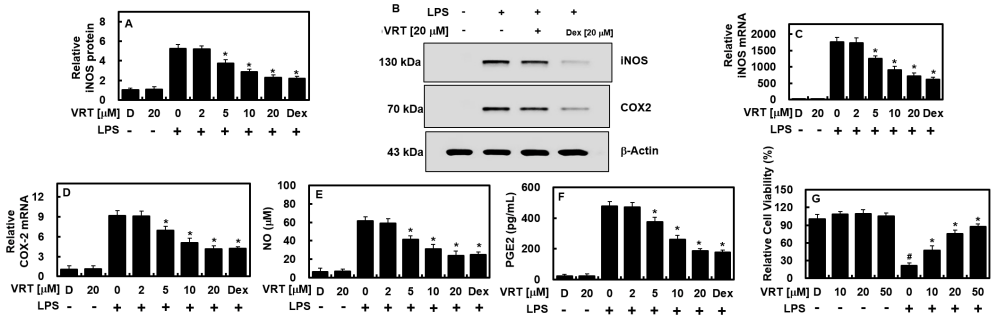

Figure 1: Treatment with VRT reduced cyclooxygenase-2 (COX-2) and inducible nitric oxide synthase (iNOS) expression in lipopolysaccharide (LPS)-stimulated human umbilical vein endothelial cells (HUVECs). Cells were initially exposed to LPS (1 μg/mL) for 6 h, followed by incubation with varying concentrations of VRT or 20 μM dexamethasone (Dex) for an additional 6 h. The measured endpoint included (**A**) iNOS protein, (**B**) COX-2 protein, (**C**) iNOS mRNA, (**D**) COX-2 mRNA, (**E**) NO, and (**F**) PGE2. Relative iNOS protein (**A**) refers to the iNOS protein levels normalized to an internal loading control. For NO quantification (**E**), levels are expressed relative to the cell culture supernatant volume. Cell viability following VRT treatment with or without LPS was determined using the MTT assay (**G**). Data represent mean ± SD from three independent experiments conducted in triplicate on separate days. The label "D" denotes 0.2% DMSO, which served as the vehicle control. $^{*}p < 0.05$ vs. LPS-treated group, while $^{\#}p < 0.05$ denotes significance compared to the DMSO control (**G**). $n = 3$.

3.2 Effect of VRT on NF-κB Activity, STAT-1 Phosphorylation, and HO-1 Protein Level in LPS-Activated HUVECs

Subsequently, the impact of VRT on the regulation of NF-κB, a pivotal transcription factor governing inflammation-related gene expression, was investigated. The data revealed that VRT inhibited NF-κB luciferase reporter activity in a dose-dependent manner, as shown in Fig. 2A. Given prior evidence implicating the janus kinase (JAK)/STAT pathway in LPS-induced upregulation of iNOS and COX-2 [26], the study further examined the effect of VRT on STAT-1 phosphorylation and related downstream signaling. Results demonstrated that VRT suppressed STAT-1 phosphorylation and its downstream effectors (Fig. 2B), while concurrently inducing a significant increase in HO-1 expression (Fig. 2C).

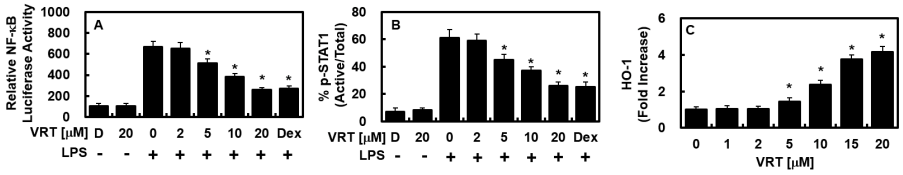

Figure 2: Treatment with VRT suppressed NF-κB and STAT-1 activities while increasing HO-1 protein expression in LPS-stimulated HUVECs. Effects of VRT on (**A**) NF-κB activity; (**B**) STAT-1 activity; (**C**) HO-1 expression. Following 6 h of LPS stimulation, cells were treated with varying concentrations of VRT or Dex (20 μM) for an additional 6 h. VRT significantly inhibited NF-κB activity, assessed using cells transfected with the NF-κB luciferase reporter vector, and reduced STAT-1 phosphorylation, measured by enzyme-linked immunosorbent assay (ELISA). Concurrently, VRT induced a dose-dependent increase in HO-1 protein levels, also quantified via ELISA from extracted cellular proteins. Data represent mean ± SD from three independent experiments conducted in triplicate on different days. The vehicle control consisted of 0.2% DMSO, denoted as "D". Statistical significance was determined at $^{*}p < 0.05$ compared to LPS-treated controls. $n = 3$.

3.3 Effects of VRT on the Nuclear Translocation Activity of Nrf2, ARE Reporter, and Anti-Inflammatory Responses

Given that the expression of HO-1 and other antioxidant enzymes depends on Nrf2 activation, we investigated the effects of VRT on Nrf2 nuclear translocation and ARE activity. The results indicated that VRT enhanced Nrf2 accumulation within the nucleus and markedly elevated ARE-luciferase reporter activity (Fig. 3A,B). To further determine whether VRT-mediated suppression of iNOS expression was associated with HO-1 induction, small interfering RNA (siRNA) targeting HO-1 was employed. Silencing HO-1 reversed the inhibitory effects of VRT, restoring iNOS and NO levels to those observed in cells lacking VRT treatment, suggesting that VRT downregulates iNOS expression through the upregulation of HO-1 (Fig. 3C,D). Consistent with these findings, VRT also demonstrated anti-inflammatory potential by reducing IL-1β levels in LPS-stimulated HUVECs (Fig. 3E).

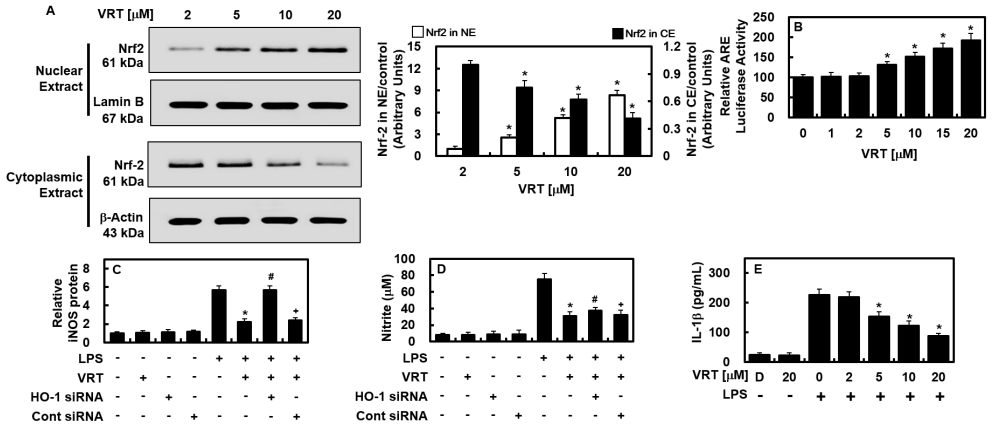

Figure 3: VRT promotes Nrf2 nuclear translocation and exerts anti-inflammatory effects in HUVECs. (**A**) Cells were incubated with increasing concentrations of VRT (2–20 μM) for 6 h, followed by separation of cytosolic and nuclear fractions. Nrf2 protein levels were quantified via Western blotting. (**B**) ARE luciferase reporter activity was assessed in lysates from cells transfected with the ARE reporter construct. (**C**,**D**) To determine the role of HO-1 induction in VRT-mediated suppression of iNOS and NO, HO-1 expression was silenced using siRNA. (E) IL-1β levels were measured by ELISA. Data represent mean ± SD from three independent experiments performed in triplicate across three separate days. Untreated control group (vehicle control) consisted of 0.2% DMSO, denoted as "D". LPS was used as a reference for comparison, and $^{*}p < 0.05$ vs. LPS, $^{\#}p < 0.05$ vs. LPS + VRT, or $^{+}p < 0.05$ vs. LPS + VRT + HO-1 siRNA. $n = 3$. Cont: Control.

3.4 Effects of VRT on TNF-α and iNOS Protein Levels in the LPS-Mediated Lung Injury Mouse Model

The anti-inflammatory potential of VRT was evaluated in animal models. As illustrated in Fig. 4A, LPS-induced elevation of TNF-α levels in bronchoalveolar lavage fluid (BALF) was significantly reduced following treatment with VRT or Dex at 0.61 mg/kg. Based on the estimated mouse blood volume (72 mL/kg) [27,28] and the body weight used in this study (27 g), the VRT doses of 0.06, 0.15, 0.30, and 0.61 mg/kg correspond to peripheral fluid concentrations of approximately 2, 5, 10, and 20 μM, respectively; Dex at 0.61 mg/kg similarly translates to 20 μM systemically. In lung tissues, iNOS expression was markedly decreased after VRT or Dex administration (Fig. 4B), confirming the *in vivo* anti-inflammatory effect of VRT. Histopathological assessments (Fig. 4C,D) revealed substantial mitigation of LPS-induced pulmonary lesions by both treatments. To further elucidate the influence of VRT on the Nrf2/HO-1 pathway and its downstream targets in mice, lung tissue mRNA expressions of Nrf2 and HO-1 were quantified, along with activities of the antioxidant enzymes catalase (CAT) and superoxide dismutase (SOD), key effectors of the

Nrf2/HO-1 axis. LPS-challenged mice exhibited significant suppression of Nrf2 and HO-1 transcripts and antioxidant enzyme activities, which were effectively restored by VRT (Fig. 4E,F and Table 1). Additionally, we assessed VRT's modulation of the Nrf2/Keap1 interaction, revealing that VRT treatment (10 and 20 μM for 6 h) disrupted Keap1-Nrf2 complex formation in HUVECs (Fig. 4G), facilitating HO-1 induction and inflammation suppression.

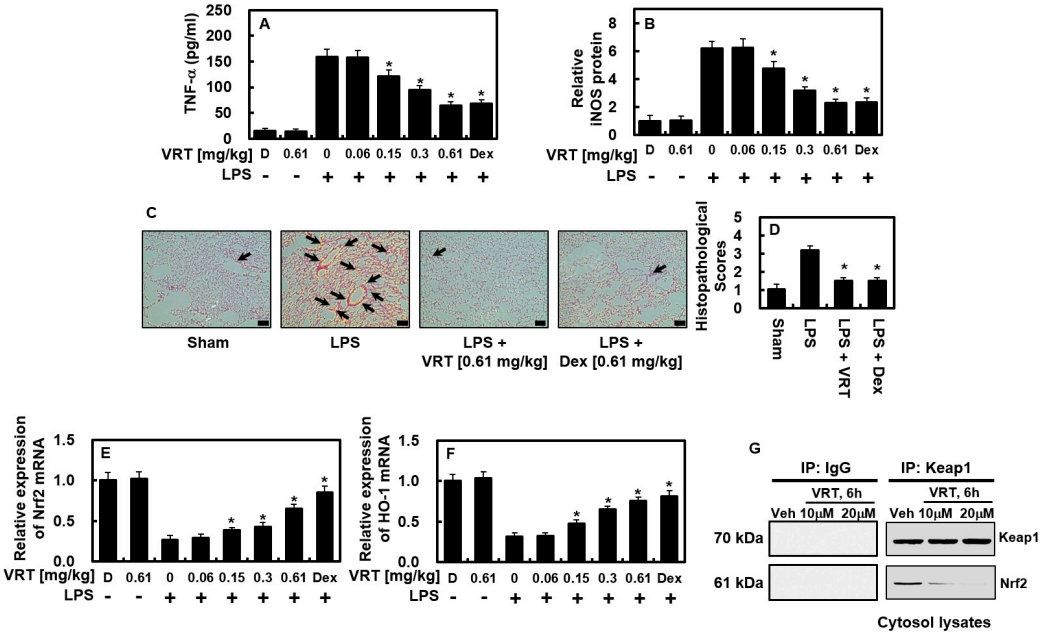

Figure 4: VRT attenuates LPS-induced lung inflammation by reducing TNF-α and iNOS levels and alleviating tissue injury in mice. Mice received intraperitoneal injection of LPS (15 mg/kg), followed 6 h later by intravenous administration of VRT (0.06–0.61 mg/kg) or Dex (0.61 mg/kg). Control mice did not receive LPS. Each experimental group consisted of five animals (n = 5). At 24 h post-LPS injection, lung tissues and bronchoalveolar lavage fluid (BALF) were collected for analysis. (**A**,**B**) Protein levels of TNF-α (**A**) and iNOS (**B**) in lung tissues. (**C**) Representative H&E-stained lung sections (scale bar: 50 μm). Arrows indicate leukocyte infiltration. Sham: control group that underwent the same experimental procedure without LPS. (**D**) Histopathological scoring of pulmonary injury as described in the Methods. (**E**,**F**) mRNA levels of Nrf2 (**E**) and HO-1 (**F**) in lung tissues. (**G**) Co-immunoprecipitation (Co-IP) assessment of Keap1-Nrf2 association in lung tissues. "D": vehicle control treated with 0.2% DMSO. Cont.: untreated control. Data represents the mean ± SD of three independent experiments, each performed in triplicate on separate days. *p < 0.05 compared with LPS-treated mice. n = 3.

Table 1: Effects of VRT treatment on the activities of antioxidant enzymes in LPS-injected mice[a].

Group	SOD (U/mg Protein)	CAT (U/mg Protein)
DMSO, mean ± SD	1.05 ± 0.03	4.19 ± 0.15
VRT (0.61 mg/kg), mean ± SD	1.04 ± 0.02	4.20 ± 0.10
LPS, mean ± SD	0.57 ± 0.05	2.72 ± 0.25
LPS + VRT (0.06 mg/kg), mean ± SD	0.58 ± 0.06	2.81 ± 0.13
LPS + VRT (0.15 mg/kg), mean ± SD	0.69 ± 0.04*	3.09 ± 0.19*
LPS + VRT (0.30 mg/kg), mean ± SD	0.79 ± 0.03*	3.75± 0.22*
LPS + VRT (0.61 mg/kg), mean ± SD	0.92 ± 0.03*	4.03 ± 0.25*

Each value represents the mean ± SD (n = 10). * p < 0.05 as compared to LPS. DMSO, dimethyl sulfoxide; VRT, veratramine; LPS, lipopolysaccharide; SOD, superoxide dismutase; CAT, Catalase.

4 Discussion

Plant-derived compounds have long been recognized as valuable modulators of inflammatory and oxidative pathways, and numerous studies in phytomedicine confirm that natural small molecules can exert potent regulatory effects on vascular and pulmonary inflammation. Polyphenols, terpenoids, flavonoids, and alkaloids—such as curcumin, quercetin, baicalin, osthole, resveratrol, and berberine—are well-documented to attenuate inflammation through activation of HO-1 or inhibition of NF-κB and STAT1 signaling [29–31]. The present findings demonstrate that VRT exhibits a similar mechanistic profile, strongly inducing HO-1 expression while suppressing iNOS, COX-2, TNF-α, and IL-1β in LPS-stimulated endothelial cells, consistent with the core principles established in botanical anti-inflammatory therapeutics. This study demonstrated that LPS stimulation significantly elevated inflammatory mediators (NO, PGE_2, TNF-α, and IL-1β) as well as regulatory enzymes (iNOS and COX-2). However, treatment with VRT effectively counteracted these increases, highlighting its potent anti-inflammatory and antioxidant activity in both LPS-stimulated cells and mice. During an inflammatory response, activated endothelial cells typically release NO, PGE_2, TNF-α, IL-1β, and the enzymes iNOS and COX-2 [32,33]. VRT markedly reduced these mediators and enzymes in vitro and in vivo, confirming its suppressive effect on inflammation. Moreover, VRT enhanced HO-1 expression in a concentration-dependent manner while attenuating COX-2/PGE_2 and iNOS/NO levels triggered by LPS and inhibiting NF-κB activity. NF-κB is a central regulator of inflammation, modulating processes such as cell adhesion, proliferation, differentiation, and apoptosis [34]. It orchestrates immune activation by promoting pro-inflammatory signaling during infection or tissue stress. Elevated NO production contributes to airway inflammation through chemokine regulation, while NF-κB activation is essential for LPS-driven iNOS and COX-2 induction. Collectively, our findings suggest that VRT mitigates LPS-induced inflammation by modulating NF-κB signaling, thereby enhancing HO-1 expression and suppressing the production of pro-inflammatory mediators (iNOS, COX-2, IL-1β, and NO). The selection of HUVECs is appropriate for this investigation since endothelial impairment is a critical factor contributing to systemic inflammation and pulmonary injury, establishing HUVECs as a suitable *in vitro* model for analyzing inflammatory signaling [35,36]. These endothelial cells enable in-depth exploration of intracellular pathways such as NF-κB, STAT1, and Nrf2, which are fundamental mediators of inflammation and oxidative reactions linked to lung tissue damage [37]. Furthermore, as human-derived cells, HUVECs generate results that better reflect human physiopathological conditions and offer a consistent, widely used system for studying endothelial activity and inflammation-related processes [35,36].

Recent publications highlight the central role of HO-1–mediated cytoprotection in phytochemical pharmacology. Natural compounds such as andrographolide, pinocembrin, luteolin, and saikosaponin A have been shown to activate the Nrf2/HO-1 axis, thereby modulating oxidative stress and regulating endothelial responses to inflammatory stimuli [38,39]. In line with these reports, our study demonstrates that VRT enhances Nrf2 translocation and HO-1 production, indicating that its anti-inflammatory efficacy occurs through a canonical antioxidative mechanism shared across many plant-derived therapeutics. This observation is further supported by the reversal of veratramine's effects upon HO-1 inhibition, validating HO-1 as a downstream mediator of its activity. The induction of HO-1 expression by VRT likely underlies the observed suppression of iNOS and TNF-α levels in the BALF of LPS-treated mice. Both current and earlier studies demonstrate that VRT stimulates HO-1, which in turn inhibits NF-κB activation and/or oxidative enzyme activity, thereby reducing substrate availability for COX2 and phosphorylation of STAT-1. Additionally, VRT enhances ARE luciferase reporter activity and promotes Nrf2 nuclear translocation. Collectively, these data indicate that VRT's anti-inflammatory properties stem from HO-1 upregulation accompanied by downregulation of iNOS expression. This mechanism is supported by RNA

interference-mediated HO-1 silencing that reverses VRT-induced suppression of NO production and iNOS expression. Accordingly, our results show that VRT upregulates HO-1 while decreasing pro-inflammatory mediators, including iNOS and TNF-α, in both LPS-stimulated HUVECs and lung tissues of LPS-injected mice. These findings highlight the pivotal role of HO-1 in mitigating inflammation, with TNF-α serving as a key effector. Furthermore, the study suggests that VRT modulates inflammatory responses through regulation of HO-1 expression, leading to inhibition of oxidase activity and/or NF-κB signaling. VRT induces HO-1 dose-dependently while suppressing NF-κB expression. Prior research has implicated activation of the Nrf2 antioxidant pathway in preventing LPS-induced transcriptional upregulation of pro-inflammatory cytokines [40]. Given that VRT effectively reduces pro-inflammatory cytokines such as TNF-α and IL-1β, it is plausible that its anti-inflammatory effects are mediated by Nrf2 pathway activation. Supporting this, VRT dose-dependently enhanced Nrf2 nuclear translocation and decreased Keap1 levels in LPS-stimulated cells, suggesting that activation of the Nrf2 antioxidant pathway is a key mechanism for VRT's therapeutic effects.

The anti-inflammatory efficacy of VRT has been extensively evaluated in animal models, producing promising outcomes. This research focused on examining VRT's effects on the protein levels of TNF-α and iNOS within a murine model of LPS-induced lung injury. Results showed a significant reduction of TNF-α concentrations in the bronchoalveolar lavage fluid (BALF) of mice after VRT administration, reflecting strong anti-inflammatory activity. Moreover, VRT substantially suppressed iNOS expression in lung tissues, further validating its anti-inflammatory potential *in vivo*. Protective effects of VRT on lung tissue integrity during inflammatory insult were also demonstrated by the attenuation of LPS-mediated pulmonary damage. These outcomes highlight VRT's therapeutic promise for inflammatory diseases, especially those involving respiratory tissues. Importantly, the administered VRT doses were converted to estimated concentrations in the peripheral fluid, offering critical insight for dosage considerations in future experimental and clinical settings. In summary, this study underscores the *in vivo* anti-inflammatory properties of VRT in lung inflammation models, supporting its candidacy for developing novel interventions against a spectrum of inflammatory disorders. Nonetheless, further investigations are required to elucidate the precise mechanisms of VRT's anti-inflammatory effects and to evaluate its potential clinical application.

VRT, as a known sodium channel modulator, may pose potential cardiovascular side effects, including alterations in cardiac conduction and rhythm disturbances such as bradycardia, arrhythmias, or even risk of heart block. Sodium channels are critical for the initiation and propagation of cardiac action potentials, so modulation by VRT could impact cardiac excitability and contractility. Although our study did not directly assess cardiovascular toxicity, these risks warrant careful consideration in future preclinical and clinical evaluations of VRT's safety profile, especially with respect to dose, duration, and patient susceptibility [11,12].

This study demonstrated that VRT facilitates the nuclear translocation of Nrf2 (Fig. 3), a central event required for activation of the Nrf2/Keap1 pathway. This was reflected by the enhanced binding of Nrf2 to antioxidant response elements (AREs) following VRT exposure. Although direct interaction between VRT and either Nrf2 or Keap1 remains to be fully validated, the observed findings strongly suggest that VRT modulates this pathway through Nrf2 stabilization or inhibition of Keap1-mediated degradation. Furthermore, VRT induced HO-1 expression—an established downstream effector of the Nrf2 pathway (Fig. 2)—providing additional mechanistic support for its role in activating the Nrf2/Keap1 axis. The suppression of inflammation via HO-1 further substantiates this regulatory link. Indeed, we confirmed that VRT (10 and 20 μM for 6 h) disrupted the Keap1-Nrf2 complex in HUVECs (Fig. 4G), reinforcing the hypothesis of direct pathway modulation.

Although this study provides meaningful insights into the anti-inflammatory potential of VRT, several important limitations should be acknowledged. First, the present investigation relied primarily on an endothelial cell–based *in vitro* model, which cannot fully recapitulate the complexity of inflammatory responses occurring in whole organisms. As such, additional *in vivo* studies are necessary to validate the physiological relevance of our findings and determine whether similar regulatory mechanisms occur in intact tissues. Second, the mechanistic analyses were limited to selected signaling pathways; other pathways known to influence endothelial inflammation may also be involved, but were not examined here. Third, the concentrations used *in vitro* may not directly reflect achievable therapeutic levels *in vivo*, and pharmacokinetic data will be required to evaluate clinical translation. Finally, the study did not assess potential off-target effects or long-term safety, which are essential considerations for therapeutic development. These limitations do not diminish the importance of the current findings but rather help define the scope of the study and identify critical directions for future investigation.

This study on the anti-inflammatory effects of VRT in lLPS-induced models provides valuable insights into its potential therapeutic role via HO-1 upregulation and modulation of Nrf2, NF-κB, and STAT1 pathways, yet several limitations merit consideration for future refinement. Primarily, the *in vitro* experiments utilized HUVECs, a well-established model for endothelial inflammation, but one that may not fully capture the intricate multicellular interactions and tissue-specific responses observed in whole organisms. The *in vivo* component employed an acute LPS-induced lung injury model in male C57BL/6 mice, which effectively demonstrates short-term protective effects but limits extrapolation to chronic inflammatory conditions, female subjects, or diverse disease etiologies beyond endotoxemia. Mechanistically, while the study robustly links VRT to Nrf2 nuclear translocation, ARE activation, and HO-1-dependent suppression of iNOS/NO and IL-1β using siRNA knockdown and reporter assays, it focuses on select pathways without comprehensively evaluating others, such as MAPK or additional JAK/STAT branches, that could contribute to its effects. Direct molecular interactions between VRT and targets like Keap1 or Nrf2 remain inferred from indirect evidence (e.g., co-IP disruption), warranting confirmatory binding studies. Pharmacologically, *in vivo* doses (0.06–0.6 mg/kg IV) were rationally scaled to *in vitro* concentrations (2–20 μM) based on estimated mouse blood volume, with no overt toxicity observed, yet formal pharmacokinetic analyses—including absorption, distribution, metabolism, excretion (ADME), and bioavailability—are absent, potentially affecting clinical translatability. Safety profiling is preliminary; as a steroidal alkaloid and known sodium channel modulator, VRT could theoretically influence cardiac excitability, though unassessed here beyond acute endpoints, suggesting a need for targeted cardiovascular evaluations in extended models. Additionally, while antioxidant enzyme activities (SOD, CAT) were restored in lung tissue, broader inflammatory markers (e.g., neutrophils in BALF, cytokines beyond TNF-α/IL-1β) were not exhaustively quantified. These aspects do not undermine the study's novel contributions—such as HO-1's mechanistic validation—but highlight opportunities for expansion, including diverse models, chronic dosing studies, comparative efficacy trials, and preclinical toxicology to strengthen VRT's candidacy for inflammation-related disorders like sepsis or vascular diseases.

Future studies should aim to delineate the precise molecular mechanisms through which VRT upregulates HO-1 and modulates both the Nrf2 and NF-κB signaling cascades. Long-term investigations are required to assess the safety profile and possible adverse effects of chronic VRT administration. Optimization of dosage regimens and delivery strategies across diverse inflammatory disease models will also be essential. Furthermore, exploring VRT's therapeutic efficacy in other inflammation-associated disorders, such as arthritis and neuroinflammation, could broaden its clinical value. Comparative analyses with established anti-inflammatory agents would help define VRT's place within current therapeutic paradigms. Ultimately,

initiating human clinical studies to evaluate VRT's pharmacokinetics, pharmacodynamics, and overall clinical tolerability will be crucial for translating it into a viable therapeutic option.

5 Conclusion

In conclusion, our findings show that VRT elevates HO-1 levels and reduces the expression of proinflammatory mediators in LPS-challenged HUVECs and lung tissues of LPS-exposed mice, including decreased iNOS and TNF-α levels. These results emphasize the critical role of HO-1 in modulating inflammatory processes and suggest a potential function of TNF-α in HO-1-mediated regulation. Collectively, VRT shows therapeutic potential for the treatment of inflammation-related diseases, particularly those affecting the respiratory system; however, its development as a clinical candidate requires further comprehensive pharmacokinetic, toxicity, and safety evaluations.

Acknowledgement: None.

Funding Statement: This research was supported by the National Research Foundation of Korea (NRF) grant funded by the Korea government (MSIT) (NRF-RS-2025-00555195).

Author Contributions: Conceptualization, methodology, investigation, Gyuri Han and Yun Hee Jeong; investigation, Ga Eun Kim; conceptualization, methodology, supervision, resources, writing—reviewing and editing, Jong-Sup Bae. All authors reviewed and approved the final version of the manuscript.

Availability of Data and Materials: The data that support the findings of this study are available from the corresponding author, upon reasonable request.

Ethics Approval: All animal procedures were approved by the Institutional Animal Care and Use Committee of Kyungpook National University (IRB No. KNU 2022-112).

Conflicts of Interest: The authors declare no conflicts of interest.

Abbreviations

ARE	antioxidant response element
COPD	chronic obstructive pulmonary disease
COX-2	cyclooxygenase-2
HO-1	heme oxygenase-1
HUVEC	human umbilical vein endothelial cell
IL	interleukin
iNOS	inducible nitric oxide synthase
LPS	lipopolysaccharide
ROS	reactive oxygen species
TNF	tumor necrosis factor
VRT	veratramine

References

1. Luu Hoang KN, Anstee JE, Arnold JN. The diverse roles of heme oxygenase-1 in tumor progression. Front Immunol. 2021;12:658315. [CrossRef].
2. Waza AA, Hamid Z, Ali S, Bhat SA, Bhat MA. A review on heme oxygenase-1 induction: is it a necessary evil. Inflammation Research. 2018;67(7):579–88. [CrossRef].
3. Su H, Wang Z, Zhou L, Liu D, Zhang N. Regulation of the Nrf2/HO-1 axis by mesenchymal stem cells-derived extracellular vesicles: Implications for disease treatment. Front Cell Dev Biol. 2024;12:1397954. [CrossRef].

4. Ngo V, Duennwald ML. Nrf2 and Oxidative Stress: a general overview of mechanisms and implications in human disease. Antioxidants. 2022;11(12):2345. [CrossRef].
5. Raghunath A, Sundarraj K, Nagarajan R, Arfuso F, Bian J, Kumar AP, et al. Antioxidant response elements: discovery, classes, regulation and potential applications. Redox Biol. 2018;17:297–314. [CrossRef].
6. Yu H, Lin L, Zhang Z, Zhang H, Hu H. Targeting NF-kappaB pathway for the therapy of diseases: Mechanism and clinical study. Signal Transduct Target Ther. 2020;5(1):209. [CrossRef].
7. Druszczynska M, Godkowicz M, Kulesza J, Wawrocki S, Fol M. Cytokine receptors-regulators of Antimycobacterial Immune Response. Int J Mol Sci. 2022;23(3):1112. [CrossRef].
8. Liu H, Yu X, Yu S, Kou J. Molecular mechanisms in lipopolysaccharide-induced pulmonary endothelial barrier dysfunction. Int Immunopharmacol. 2015;29(2):937–46. [CrossRef].
9. Abdel-Aziz S, Aeron A, Kahil T. Health benefits and possible risks of herbal medicine. In: Microbes in food and health. Berlin/Heidelberg, Germany: Springer; 2016. p. 97–116. [CrossRef].
10. Li Q, Zhao YL, Long CB, Zhu PF, Liu YP, Luo XD. Seven new veratramine-type alkaloids with potent analgesic effect from Veratrum taliense. J Ethnopharmacol. 2019;244:112137. [CrossRef].
11. Wang L, Li W, Liu Y. Hypotensive effect and toxicology of total alkaloids and veratramine from roots and rhizomes of *Veratrum nigrum* L. in spontaneously hypertensive rats. Pharmazie. 2008;63(8):606–10.
12. Zhou Z, Chen J, Cui Y, Zhao R, Wang H, Yu R, et al. Antihypertensive activity of different components of *Veratrum* alkaloids through metabonomic data analysis. Phytomedicine. 2023;120:155033. [CrossRef].
13. Yin L, Xia Y, Xu P, Zheng W, Gao Y, Xie F, et al. Veratramine suppresses human HepG2 liver cancer cell growth *in vitro* and *in vivo* by inducing autophagic cell death. Oncol Rep. 2020;44(2):477–86. [CrossRef].
14. Zhang Y, Ye G, Chen Y, Sheng C, Wang J, Kong L, et al. Veratramine ameliorates pain symptoms in rats with diabetic peripheral neuropathy by inhibiting activation of the SIGMAR1-NMDAR pathway. Pharm Biol. 2022;60(1):2145–54. [CrossRef].
15. Hong SS, Lee JY, Jeong YW, Lee JE, Choi YH, Jeong W, et al. Phytochemical investigation on the aerial parts of *Veratrum versicolor* f. *viride Nakai* and their biological activities. Turk J Chem. 2023;47(6):1346–54. [CrossRef].
16. Li Q, Yang KX, Zhao YL, Qin XJ, Yang XW, Liu L, et al. Potent anti-inflammatory and analgesic steroidal alkaloids from *Veratrum taliense*. J Ethnopharmacol. 2016;179:274–9. [CrossRef].
17. Kim C, Ryu SH, Kim N, Lee W, Bae J-S. Renal protective effects of sparstolonin b in a mouse model of sepsis. Biotechnol Bioprocess Eng. 2022;27(2):157–62. [CrossRef].
18. Baek DH, Kim GO, Choi HJ, Yun MY, Park DH, Song GY, et al. Inhibitory activities of GDX-365 on HMGB1-mediated septic responses. Biotechnol Bioprocess Eng. 2023;28(4):623–31. [CrossRef].
19. Kim C, Ryu SH, Choi H, Park DH, Bae JS. The inhibitory functions of sparstolonin B against ambient fine particulate matter induced lung injury. Biotechnol Bioprocess Eng. 2022;27(6):949–60. [CrossRef].
20. David S, Ghosh CC, Kumpers P, Shushakova N, Van Slyke P, Khankin EV, et al. Effects of a synthetic PEG-ylated Tie-2 agonist peptide on endotoxemic lung injury and mortality. Am J Physiol Lung Cell Mol Physiol. 2011;300(6):L851–62. [CrossRef].
21. Fu X, Ju J, Lin Z, Xiao W, Li X, Zhuang B, et al. Target deletion of complement component 9 attenuates antibody-mediated hemolysis and lipopolysaccharide (LPS)-induced acute shock in mice. Sci Rep. 2016;6:30239. [CrossRef].
22. Lee I-C, Bae J-S. Hepatic protective effects of jujuboside B through the modulation of inflammatory pathways. Biotechnol Bioprocess Eng. 2022;27(3):336–43. [CrossRef].
23. Lee WH, Choo S, Sim H, Bae JS. Inhibitory activities of ononin on particulate matter-induced oxidative stress. Biotechnol Bioprocess Eng. 2021;26(2):208–15. [CrossRef].
24. Kim JE, Lee W, Yang S, Cho SH, Baek MC, Song GY, et al. Suppressive effects of rare ginsenosides, Rk1 and Rg5, on HMGB1-mediated septic responses. Food Chem Toxicol. 2019;124:45–53. [CrossRef].
25. Lee W, Ku SK, Kim JE, Cho GE, Song GY, Bae JS. Pulmonary protective functions of rare ginsenoside Rg4 on particulate matter-induced inflammatory responses. Biotechnol Bioprocess Eng. 2019;24(3):445–53. [CrossRef].
26. Kim TW, Shin JS, Chung KS, Lee YG, Baek NI, Lee KT. Anti-inflammatory mechanisms of koreanaside A, a lignan isolated from the flower of forsythia koreana, against LPS-induced macrophage activation and DSS-induced colitis mice: The crucial role of AP-1, NF-kappaB, and JAK/STAT signaling. Cells. 2019;8(10):1163. [CrossRef].

27. Lee W, Lee D, Lee Y, Lee T, Song KS, Yang EJ, et al. Isolation, synthesis, and antisepsis effects of a C-methylcoumarinochromone isolated from abronia nana cell culture. J Nat Prod. 2018;81(5):1173–82. [CrossRef].
28. Lee W, Park SY, Yoo Y, Kim SY, Kim JE, Kim SW, et al. Macrophagic Stabilin-1 restored disruption of vascular integrity caused by sepsis. Thromb Haemost. 2018;118(10):1776–89. [CrossRef].
29. Hahn D, Shin SH, Bae JS. Natural antioxidant and anti-inflammatory compounds in foodstuff or medicinal herbs inducing heme Oxygenase-1 expression. Antioxidants. 2020;9(12):1191. [CrossRef].
30. Choy KW, Murugan D, Leong XF, Abas R, Alias A, Mustafa MR. Flavonoids as natural anti-inflammatory agents targeting nuclear factor-kappa B (NFκB) signaling in cardiovascular diseases: a mini review. Front Pharmacol. 2019;10:1295. [CrossRef].
31. Kushwaha R, Alugoju P, Anthikapalli NVA, Sharma R, Sedlarova M, Pospisil P, et al. Bioactive compounds in the modulation of oxidative stress in monocytes and macrophages. Sci Rep. 2025;15(1):32012. [CrossRef].
32. McInnes IB, Schett G. The pathogenesis of rheumatoid arthritis. N Engl J Med. 2011;365(23):2205–19. [CrossRef].
33. Gaddi A, Cicero AF, Pedro EJ. Clinical perspectives of anti-inflammatory therapy in the elderly: the lipoxigenase (LOX)/cycloxigenase (COX) inhibition concept. Arch Gerontol Geriatr. 2004;38(3):201–12. [CrossRef].
34. Wullaert A, Bonnet MC, Pasparakis M. NF-kappaB in the regulation of epithelial homeostasis and inflammation. Cell Research. 2011;21(1):146–58. [CrossRef].
35. Halaidych OV, Freund C, van den Hil F, Salvatori DCF, Riminucci M, Mummery CL, et al. Inflammatory responses and barrier function of endothelial cells derived from human induced pluripotent stem cells. Stem Cell Rep. 2018;10(5):1642–56. [CrossRef].
36. Kocherova I, Bryja A, Mozdziak P, Angelova Volponi A, Dyszkiewicz-Konwinska M, Piotrowska-Kempisty H, et al. Human umbilical vein endothelial cells (HUVECs) co-culture with osteogenic cells: from molecular communication to engineering prevascularised bone grafts. J Clin Med. 2019;8(10):1602. [CrossRef].
37. Guo Q, Jin Y, Chen X, Ye X, Shen X, Lin M, et al. NF-kappaB in biology and targeted therapy: new insights and translational implications. Signal Transduct Target Ther. 2024;9(1):53. [CrossRef].
38. Ge J, Liu Z, Zhong Z, Wang L, Zhuo X, Li J, et al. Natural terpenoids with anti-inflammatory activities: potential leads for anti-inflammatory drug discovery. Bioorg Chem. 2022;124:105817. [CrossRef].
39. Huang Z, Wu M, Zeng L, Wang D. The beneficial role of Nrf2 in the endothelial dysfunction of atherosclerosis. Cardiol Res Pract. 2022;2022(1):4287711. [CrossRef].
40. Ahmed SM, Luo L, Namani A, Wang XJ, Tang X. Nrf2 signaling pathway: pivotal roles in inflammation. Biochim Biophys Acta Mol Basis Dis. 2017;1863(2):585–97. [CrossRef].